Journal of Sound and Vibration (1999) **221**(4), 623–649
Article No. jsvi.1998.2032, available online at http://www.idealibrary.com on IDEAL

ON THE BENDING COUPLED NATURAL FREQUENCIES OF A SPINNING, MULTISPAN TIMOSHENKO SHAFT CARRYING ELASTIC DISKS

H. S. JIA
Department of Mechanical Engineering, University of Toronto, 5 King's College Road, Toronto, Ontario M5S 3G8, Canada

(*Received* 17 *June* 1998, *and in final form* 19 *October* 1998)

Vibration problems of spinning shafts with attached disks occur quite frequently, but until recently the analyses were generally restricted to the flexible-shaft/rigid-disk models, which lost at least two-thirds of the vibrational characteristics to a certain extent. In the present paper, a substructure synthesis technique is applied to the modelling of the bending coupled dynamics of a spinning shaft/disk system with disk flexibility considered. The shaft is treated as a Timoshenko beam. The coupled equations of motion are derived analytically. A numerical study is performed to demonstrate the method developed. The bending coupled natural frequencies, both in view of the shaft transverse vibration and in view of the disk transverse vibration, and the coupled mode shapes are obtained as spin speed varies. The disk flexibility has important effects on the system vibrational behavior, especially at the frequency range near the natural frequencies of single disks.

1. INTRODUCTION

The vibrations of a spinning shaft with attached disks are of wide research interest as an essential element of many modern machines. The analysis is generally restricted to the flexible-shaft/rigid-disk model. In another aspect, there has been extensive research on the vibrations of flexible disks since the famous early works [1–5]. A single disk with inner-clamped and outer-free boundaries can be modelled as an elastic disk rigidly attached to a rigid shaft with rigid bearings. For the two models above, no flexible coupling effects exist between the disks and the shaft in addition to the rigid rotation effects—the rotary inertia effect and the gyroscopic moments. The present research will show that for an elastic shaft/disk structure, the coupled vibrations consist of shaft-dominating modes, disk-dominating modes and shaft–disk coupled modes. The flexible-shaft/rigid-disk model can only predict the shaft-dominating modes with some frequency values over-estimated, while leaving the disk-dominating modes and shaft-disk coupled modes unperceived. So, to a certain extent, at least two-thirds of the vibratory characteristics are lost when analyzed relying on a shaft/rigid-disk model.

0022–460X/99/040623 + 27 $30.00/0

According to the nature of coupling with the shaft, disk vibratory modes are classified for convenience into three groups (section 2.3): uncoupled disk modes with more than one nodal diameter, disk modes with a single nodal diameter coupled with the shaft bending vibrations and disk modes with zero nodal diameter (axisymmetric modes) coupled with the shaft longitudinal (axial) vibrations. The uncoupled disk modes can be calculated accurately, if the accurate values of Bessel functions are available, for stationary disks, or by approximate methods for rotating disks or disks containing radially symmetric stress fields, arising, for example, from residual or thermal effects [6]. The longitudinal coupled vibrations were addressed by Jia *et al*. [7]. Several investigators have modelled the bending coupled vibrations based on different schemes, which are summarized as follows. Dopkin and Shoup [8] analyzed the effect of disk flexibility and gyroscopic forces on the bending natural frequencies of an axisymmetric rotating shaft with flexible disks by a transfer matrix analysis. Chivens and Nelson [9] analytically investigated the influence of disk flexibility on both the natural frequencies and critical speeds of a flexible shaft–disk system. Wilgen and Schlack [10] applied the Liapunov method to an analysis model consisting of a flexible disk rigidly attached at an arbitrary location along a flexible shaft to investigate the effects of disk flexibility on the stability. Shahab and Thomas [11] studied the coupling behavior between the stationary flexible thick disks and the flexible shaft carrying these disks by a finite element method. Vance [12] considered the attachment flexibility of the disks to the shaft. Wu and Flowers [13] developed a transfer matrix procedure in which the disk flexibility effects were accounted for by means of additional terms included in the transfer matrix formulation. Shen and Ku [14] suggested an analytical formulation for a rigid spindle with elastic circular disk supported by two elastic antifriction bearings to predict the non-traditional vibration resonances encountered in modern disk drives.

In this paper, the bending coupled vibrations of a flexible shaft–flexible disk system are studied by a substructure synthesis technique [15]. The method has been successfully applied to predict the tricky coupled vibrations of commercial computer hard disk drive spindle systems [16] where the flexible shaft was modelled as a Rayleigh beam [17] in which the lateral motion and the rotary inertia effect are considered, but the shear deformation effect is neglected. For the present work, the method is further developed to apply to a multispan Timoshenko beam [18, 19], in which both the rotary inertia effect and the shear deformation effect of the elastic shaft are taken into account, with elastic circular disks. In addition, multiple isotropic journal bearings are included.

2. MODELLING ASSUMPTIONS AND ANALYSIS METHOD

2.1. ASSUMPTIONS

The system to be analyzed, shown in Figure 1, consists of a flexible shaft carrying M flexible disks rigidly attached to the shaft. The assumption of rigid attachment means that the inner boundary of the disks remains normal to the

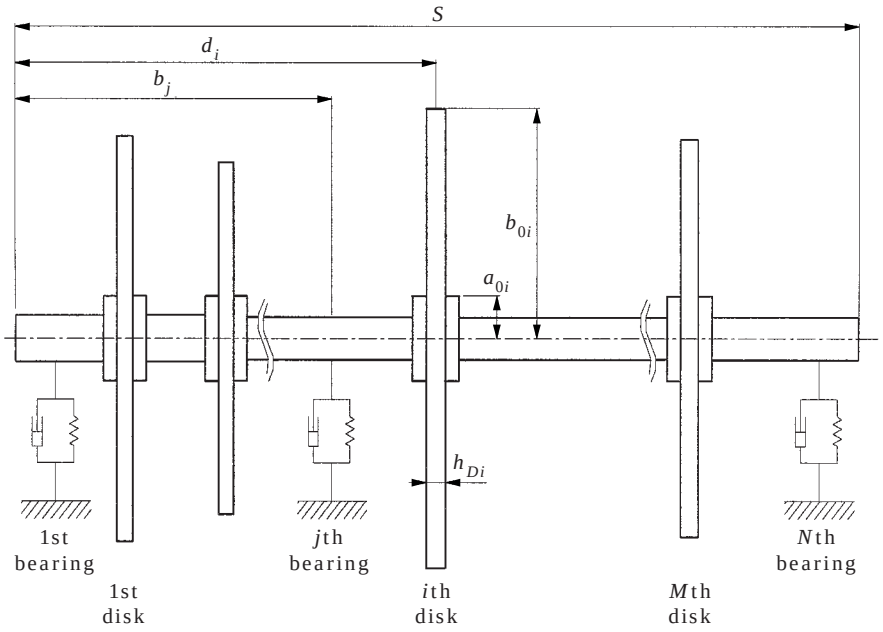

Figure 1. Analysis model.

shaft in all modes. The shaft is supported by N flexible journal bearings. It is assumed that the shaft is of varying annular cross-section and each disk is a uniform circular plate, as used for steam turbines.

The shaft is modelled as a Timoshenko beam, considering rotary inertia and shear deformation effects.

The classical thin plate theory or Kirchhoff plate theory [20] is used to describe the disk vibration, where the non-linear effect and the thick plate effects of rotary inertia and shear deformations are neglected. The normals to the middle plane of the plate are assumed to remain normal to the deflected middle plane during vibration, and the dissipation due to damping is not included. The centrifugal stiffening effect of the disk is included.

The gyroscopic or Coriolis effect is included. Small deformation is assumed throughout the analysis. The bending coupled vibrations of the system will be analyzed. In particular, a few lowest vibration modes are of major interest.

2.2. CO-ORDINATE SYSTEMS

In order to obtain the total kinetic and potential energies, the system may be conveniently regarded as an assemblage of substructures to which local reference frames are assigned to describe the rigid body motions. Then, elastic deformations are defined as motions relative to the moving local reference frames. Three co-ordinate systems are used (see Figure 2). An $X_0-Y_0-Z_0$ frame represents the inertial (Newtonian) system; $X_1-Y_1-Z_1$ is the local reference frame rotating at the shaft angular speed Ω about the X_1 axis, where the X_0 and X_1 axes are collinear and coincident with the undeformed bearing centerline; $X_2-Y_2-Z_2$ is the local reference frame fixed to a disk with the origin at the center of

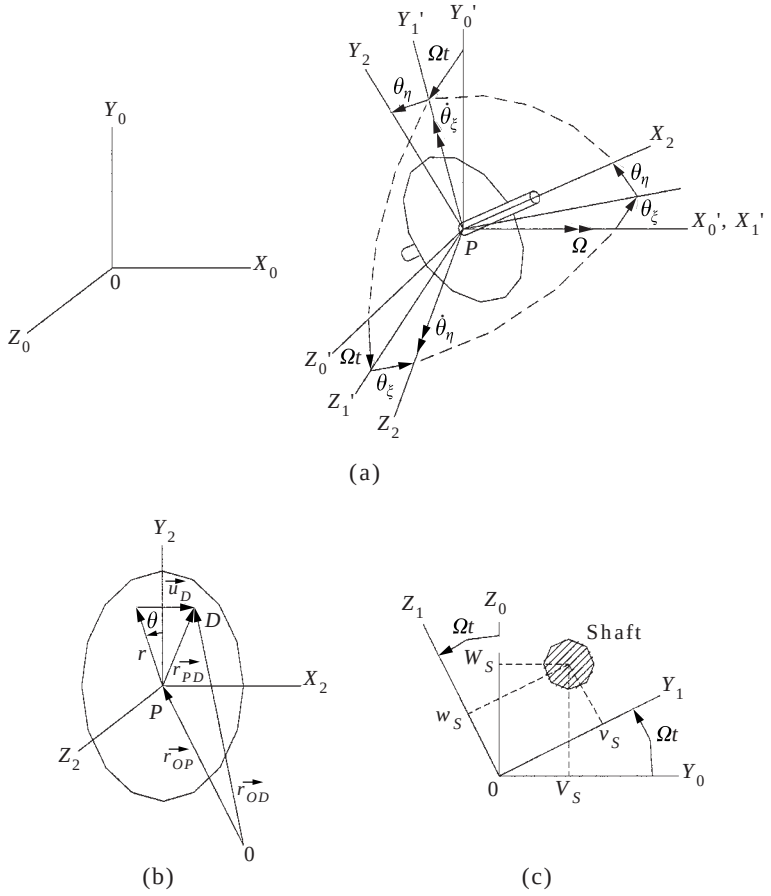

Figure 2. Co-ordinate systems: (a) the rigid body motion of a disk, (b) the flexible transverse deformation of a disk, and (c) the lateral deformation of the shaft.

the disk. The whirling of the shaft is represented by (v_S, w_S) in X_1–Y_1–Z_1. The elastic deflection of the disk relative to X_2–Y_2–Z_2 is denoted by u_D. The rigid body rotation of the disk is defined by first the rotation Ωt about X_0', then the small rotation angle θ_ξ about Y_1', and last, the small rotation angle θ_η about Z_2.

2.3. COUPLING ANALYSIS OF A ELASTIC SHAFT–DISK STRUCTURE

To investigate the coupling caused by disk flexibility, one chooses a section (Figure 3) including one disk from the shaft/multiple-disk system. It is assumed that the attachment of the disk to the shaft is rigid, so that the disk remains normal to the shaft in all modes. For a rotating uniform disk, the differential equation of elastic transverse vibration can be derived by the application of Hamilton's principle. The equation of free vibration has the form

$$\rho_D h_D \frac{\partial^2 u_D}{\partial t^2} + D\nabla^4 u_D - \frac{1}{r}\frac{\partial}{\partial r}\left(rN_r \frac{\partial u_D}{\partial r}\right) - \frac{1}{r^2} N_\theta \frac{\partial^2 u_D}{\partial \theta^2} = 0, \tag{1}$$

with the inner-clamped boundary conditions

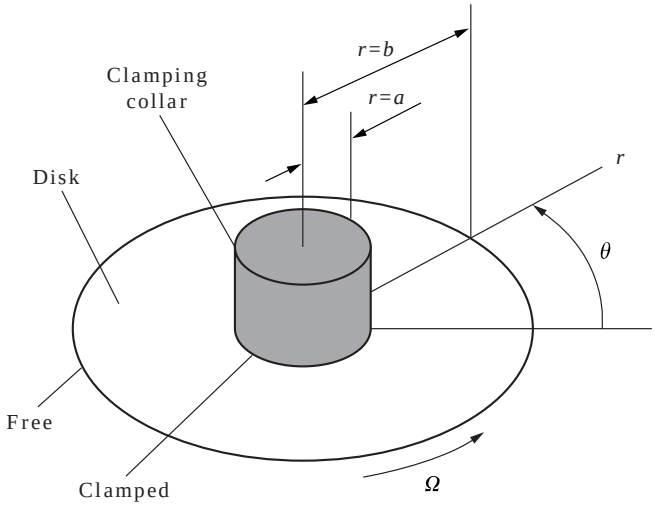

Figure 3. Analysis model for shaft/flexible-disk coupling.

$$u_D|_{r=a} = 0, \quad \left.\frac{\partial u_D}{\partial r}\right|_{r=a} = 0, \tag{2}$$

and the outer-free boundary conditions

$$\left[\frac{\partial^2 u_D}{\partial^2 r} + v_D\left(\frac{1}{r}\frac{\partial u_D}{\partial r} + \frac{1}{r^2}\frac{\partial^2 u_D}{\partial \theta^2}\right)\right]\Bigg|_{r=b} = 0,$$
$$\left[\frac{\partial}{\partial r}\nabla^2 u_D + \frac{(1-v_D)}{r^2}\frac{\partial^2}{\partial \theta^2}\left(\frac{\partial u_D}{\partial r} - \frac{u_D}{r}\right)\right]\Bigg|_{r=b} = 0, \tag{3}$$

where a and b are the inner and outer radii of the disk, respectively; ρ_D is the mass per unit volume of the disk, h_D is the thickness of the disk; D is the flexural rigidity of the disk; v_D is the Poisson's ratio; ∇^4 is the biharmonic operator ($\nabla^4 u_D = \nabla^2(\nabla^2 u_D)$); N_r and N_θ are normal stress resultants in polar coordinates; ∇^2 is the Laplacian operator. The expressions are detailed in Appendix A, where Ω is the constant rotating speed of the shaft (rad/s) and E_D is the Young's modulus.

Considering the derivation by Meirovitch [21] and

$$\int_0^{2\pi}\int_a^b uL[v]r\,\mathrm{d}\,r\,\mathrm{d}\,\theta = \int_0^{2\pi}\int_a^b\left(N_r\frac{\partial u}{\partial r}\frac{\partial v}{\partial r} + \frac{N_\theta}{r^2}\frac{\partial u}{\partial \theta}\frac{\partial v}{\partial \theta}\right)r\,\mathrm{d}\,r\,\mathrm{d}\,\theta,$$

where

$$L = -\frac{1}{r}\frac{\partial}{\partial r}\left(rN_r\frac{\partial}{\partial r}\right) - \frac{1}{r^2}N_\theta\frac{\partial^2}{\partial \theta^2},$$

and u and v are two arbitrary comparison functions, it is straightforward to demonstrate that the eigenvalue problem for the elastic transverse vibration (1)–

(3) of a uniform disk is self-adjoint, and it follows that its eigenfunctions constitute a complete set of orthogonal modes. Then, the flexible displacement of the elastic disk can be expressed according to the expansion theorem

$$u_D(r,\theta,t) = \sum_{i=1}^{\infty} U_i(r,\theta) q_i(t),$$

where $U_i(r,\theta)$ are orthonormal modes of the disk, and $q_i(t)$ are the corresponding time-dependent generalized co-ordinates. Here one considers harmonic vibration, so that $\ddot{q}_i(t) = -\omega_i^2 q_i(t)$, where ω_i is the natural frequency of the ith disk mode and a dot denotes derivative with respect to time t. $U_i(r,\theta)$ may be expressed in the form [4]

$$U_i(r,\theta) = U_{mn}(r,\theta) = R_{mn}(r)(a_{mn}\cos m\theta + b_{mn}\sin m\theta), \qquad m,n = 0,1,2,\ldots,\infty,$$

where $U_{mn}(r,\theta)$ represent the orthonormal modes of m nodal diameters and n nodal circles. $U_i(r,\theta)$ can be regarded as the reranking of $U_{mn}(r,\theta)$ by order of increasing corresponding natural frequencies. $R_{mn}(r)$ is the radial distribution of the mode shape. a_{mn} and b_{mn} are constants determining the orientation angle θ_{mn0} of the resultant mode relative to the disk: $a_{mn}\cos m\theta + b_{mn}\sin m\theta = \cos m(\theta + \theta_{mn0})$. For a perfectly symmetric disk, whether uniform or not, theory indicates, and experiment verifies, that there will be no fixed preferential orientation (θ_{mn0}) of the mode with respect to the disk (reference [17], pp. 363–366). Therefore, to simplify the following formulation, without loss of generality, it is assumed that $\theta_{mn0} = 0$.

The inertia force of the vibrating disk is

$$F_P = -\rho_D h_D \int_0^{2\pi}\int_a^b \frac{\partial^2 u_D}{\partial t^2} r\,\mathrm{d}r\,\mathrm{d}\theta$$

$$= -\rho_D h_D \sum_{i=1}^{\infty} \omega_i^2 q_i(t) \int_0^{2\pi}\int_a^b R_{mn}(r)\,\cos(m\theta) r\,\mathrm{d}r\,\mathrm{d}\theta,$$

where

$$\int_0^{2\pi} \cos(m\theta)\,\mathrm{d}\theta = \begin{cases} 2\pi, & \text{for } m = 0, \\ 0, & \text{for } m \neq 0. \end{cases} \tag{4}$$

And the inertia moment about P (the direction is perpendicular to the shaft) is

$$M_P = -\rho_D h_D \int_0^{2\pi}\int_a^b \frac{\partial^2 u_D}{\partial t^2} r\cos\theta r\,\mathrm{d}r\,\mathrm{d}\theta$$

$$= -\rho_D h_D \sum_{i=1}^{\infty} \omega_i^2 q_i(t) \int_0^{2\pi}\int_a^b R_{mn}(r)\cos(m\theta)\cos\theta r^2\,\mathrm{d}r\,\mathrm{d}\theta,$$

where

$$\int_0^{2\pi} \cos(m\theta)\,\cos\,\theta\,\mathrm{d}\theta = \begin{cases} \pi, & \text{for } m = 1, \\ 0, & \text{for } m \neq 1. \end{cases} \tag{5}$$

Formulas (4) and (5) imply that the disk modes of zero nodal diameter (axisymmetric modes) couple with the longitudinal vibration of the shaft for the inertia force F_p, the disk modes of one nodal diameter couple with the bending vibration of the shaft for the inertia moment M_p, and all other modes of nodal diameter $m \geqslant 2$ do not couple with the shaft vibration. Accordingly, in the following discussion of bending coupled vibrations, only disk modes of single nodal diameter are considered, and the disk modes appearing in the ensuing paragraph, unless otherwise specified, are modes of single nodal diameter.

2.4. SUBSTRUCTURE SYNTHESIS

A substructure synthesis technique, developed for the modelling of flexible multibody systems, is used to investigate the coupled vibrations of the flexible disk/shaft/bearing system. The total system is regarded as a disconnected assemblage of substructures (flexible shaft and flexible disks) which satisfy the geometric constraint conditions of motion at the disconnected points. The energy functions for every substructure are determined by elastic deformations and fictitious geometric constraint conditions. The motion of every substructure is represented as a weighted finite series of admissible functions (assumed modes method). As admissible functions, the mode shapes obtained from the analytical solutions of individual non-rotating elements can be used. The energy elements are obtained in a discretized form by expressing motions in terms of the weighted admissible functions. Then, Lagrange's equations of motion are used to formulate the equations of motion. Compared with the popular FEM (finite element method) in complex mechanical and structural vibration analysis, several observations can be made:

(1) The substructure synthesis method does not need the large number of degrees of freedom as required in finite element analysis.

(2) Due to the expansion in terms of the global admissible functions, which extend over the entire individual substructures in substructure synthesis, the fundamental vibration characteristics of the system is ensured to be correct, since the admissible functions consist of one set of approximate solutions of the system. In contrast, the FEM, which uses local admissible functions defined over small subdomains of substructures, might lead to erroneous numerical output in dynamic problems of continuous media.

(3) However, the substructure synthesis method is applicable to relatively regular systems, consisting of simple structural elements (substructures), such as beams and plates, the exact analytic mode shapes of which are well available, while the FEM is applicable to irregular systems. This restriction to substructure synthesis is not an excessive demand considering that most practical structures can be idealized as composed of simple substructures.

3. GOVERNING EQUATIONS

3.1. ENERGY FUNCTIONS

The goal of the following analysis is to produce equations governing the transverse bending coupled vibrations of a flexible shaft/disks system based on a Timoshenko beam model. The substructure synthesis technique is applied to discretize the complex continuous structure. For the bending coupled vibration of the shaft and the single nodal diameter disk modes, in addition to the transverse displacements, the gyroscopic moments, and rotary inertia and shear deformation effects are considered.

The fundamental assumption in the bending analysis of the shaft including shear deflection is that plane cross-sections originally normal to the neutral axis remain plane, but they do not remain normal to the deformed neutral axis.

Four independent variables are needed to describe the shaft transverse motion in two orthogonal planes in the rotating co-ordinates X_1–Y_1–Z_1: v_{S1} and w_{S1}, and v_{S1} and w_{S2}, where v_{S1} and w_{S1} are small transverse deflections due to bending (flexure), and v_{S2} and w_{S2} are small transverse deflections due to shearing. Then, the total transverse deflections are

$$v_S = v_{S1} + v_{S2}, \quad w_S = w_{S1} + w_{S2}.$$

The potential energy, V_S, of the shaft due to the shearing and bending deformations in the rotating co-ordinate system, X_1–Y_1–Z_1, is expressed as [22]

$$V_s = \frac{1}{2}\int_0^S \left\{ kG_S A_S \left[\left(\frac{\partial v_{S2}}{\partial x}\right)^2 + \left(\frac{\partial w_{S2}}{\partial x}\right)^2 \right] + E_S I_S \left[\left(\frac{\partial^2 v_{S1}}{\partial x^2}\right)^2 + \left(\frac{\partial^2 w_{S1}}{\partial x^2}\right)^2 \right] \right\} \mathrm{d}x, \tag{6}$$

where k is the shear correction factor (or shape factor, since it is a function of the cross-sectional shape) which is introduced to consider the non-uniform shear stress distribution over the cross-sectional area (Timoshenko's hypothesis results in a uniform shear strain); E_S, G_S, and A_S are the Young's modulus, shear modulus and cross-sectional area of the shaft, respectively; and I_S is the area moment of inertia of the shaft about a diameter.

The kinetic energy of the shaft is due to translation and rotation and is written as [23]

$$\begin{aligned} T_S(t) = {} & \frac{1}{2}\int_0^S \rho_S A_S [\dot{v}_S^2 + \dot{w}_S^2 + 2\Omega(\dot{w}_S v_S - \dot{v}_S w_S) + \Omega^2(v_S^2 + w_S^2)]\,\mathrm{d}x \\ & + \frac{1}{2}\int_0^S \rho_S I_S [\dot{\theta}_{S\xi}^2 + \dot{\theta}_{S\eta}^2 + 2\Omega(\dot{\theta}_{S\eta}\theta_{S\xi} + \dot{\theta}_{S\xi}\theta_{S\eta}) - \Omega^2(\theta_{S\xi}^2 + \theta_{S\eta}^2)]\,\mathrm{d}x \\ & + \int_0^S \rho_S I_S \Omega^2\,\mathrm{d}x, \end{aligned} \tag{7}$$

where $\theta_{S\xi}$ and $\theta_{S\eta}$ are small angles of rotation of the shaft cross-section due to

bending, and may be expressed as

$$\theta_{S\xi} = -\frac{\partial w_{S1}}{\partial x} \quad \text{and} \quad \theta_{S\eta} = \frac{\partial v_{S1}}{\partial x}.$$

The kinetic energy of the ith disk is

$$\begin{aligned} T_{Di} = {} & \frac{1}{2} m_{Di}\{\dot{v}_i^2 + \dot{w}_i^2 + 2\Omega(\dot{w}_i v_i - \dot{v}_i w_i) + \Omega^2(v_i^2 + w_i^2)\} \\ & + \frac{1}{2} J_{Dyi}\{(\dot{\theta}_{\xi i} - \Omega\theta_{\eta i})^2 + (\dot{\theta}_{\eta i} + \Omega\theta_{\xi i})^2\} \\ & + \frac{1}{2} J_{Dxi}\{2\Omega\theta_{\eta i}\dot{\theta}_{\xi i} - \Omega^2(\theta_{\eta i}^2 + \theta_{\xi i}^2) + \Omega^2\} \\ & + \frac{1}{2}\rho_D h_{Di}\int_0^{2\pi}\int_{a_{0i}}^{b_{0i}}\{\dot{u}_{Di}^2 + 2r[\sin\theta(\dot{\theta}_{\xi i} - \Omega\theta_{\eta i}) - \cos\theta(\dot{\theta}_{\eta i} + \Omega\theta_{\xi i})]\dot{u}_{Di} \\ & - 2\Omega r[(\dot{\theta}_{\eta i} + \Omega\theta_{\xi i})\sin\theta + (\dot{\theta}_{\xi i} - \Omega\theta_{\eta i})\cos\theta]u_{Di}\} r\,\mathrm{d}r\,\mathrm{d}\theta, \end{aligned}$$

where a_{0i} and b_{0i} are the inner and outer radii, respectively; h_{Di} is the thickness; m_{Di} is the mass; J_{Dxi} and J_{Dyi} are the disk mass moments of inertia about the axis of rotation and a diameter, respectively; v_i and w_i are the shaft displacements at the ith disk location; and $\theta_{\xi i}$ and $\theta_{\eta i}$ are the small rotation angles due to bending of the shaft at the ith disk location. Note that the energy terms associated with the constant rigid body rotation are neglected since they will subsequently be cancelled out in Lagrange's equations.

The strain energy of the ith disk can be expressed as [7]

$$\begin{aligned} V_{Di}(t) = {} & \frac{D_i}{2}\int_0^{2\pi}\int_{a_{0i}}^{b_{0i}}\left\{(\nabla^2 u_{Di})^2 - 2(1-\nu_D)\frac{\partial^2 u_{Di}}{\partial r^2}\left(\frac{1}{r}\frac{\partial u_{Di}}{\partial r} + \frac{1}{r^2}\frac{\partial^2 u_{Di}}{\partial\theta^2}\right)\right. \\ & \left. + 2(1-\nu_D)\left[\frac{\partial}{\partial r}\left(\frac{1}{r}\frac{\partial u_{Di}}{\partial\theta}\right)\right]^2\right\} r\,\mathrm{d}r\,\mathrm{d}\theta \\ & + \frac{1}{2}\int_0^{2\pi}\int_{a_{0i}}^{b_{0i}}\left[N_r\left(\frac{\partial u_{Di}}{\partial r}\right)^2 + N_\theta\left(\frac{1}{r}\frac{\partial u_{Di}}{\partial\theta}\right)^2\right] r\,\mathrm{d}r\,\mathrm{d}\theta, \end{aligned}$$

The total kinetic and potential energy of the disks are respectively

$$T_D = \sum_{i=1}^{M} T_{Di}, \quad V_D = \sum_{i=1}^{M} V_{Di}. \tag{8}$$

To introduce the bearing forces, one makes use of the virtual work expression

$$\begin{aligned} \delta W(t) = \sum_{i=1}^{N}[& -(k_{iyy}V_S + k_{iyz}W_S + c_{iyy}\dot{V}_S + c_{iyz}\dot{W}_S)\delta V_S \\ & - (k_{izy}V_S + k_{izz}W_S + c_{izy}\dot{V}_S + c_{izz}\dot{W}_S)\delta W_S]|_{bi}. \end{aligned}$$

where $|_{bi}$ represents that the shaft displacements are evaluated at the ith bearing location, and V_S and W_S are shaft deflections in the inertial co-ordinate system X_0–Y_0–Z_0. One assumes that $k_{iyy} = k_{izz} = k_{i1}$, $k_{iyz} = -k_{izy} = k_{i2}$, $c_{iyy} = c_{izz} = c_{i1}$,

and $c_{iyz} = -c_{izy} = c_{i2}$ (sufficient but not essential conditions for isotropic bearings). Then

$$\delta W(t) = \sum_{i=1}^{N} [-(k_{i1} V_S + k_{i2} W_S + c_{i1} \dot{V}_S + c_{i2} \dot{W}_S)\delta V_S - (-k_{i2} V_S + k_{i1} W_S - c_{i2} \dot{V}_S + c_{i1} \dot{W}_S)\delta W_S]|_{bi}. \tag{9}$$

The relations between displacements v_S, w_S and V_S, W_S are given by

$$V_S = v_S \cos \Omega t - w_S \sin \Omega t, \quad W_S = v_S \sin \Omega t + w_S \cos \Omega t, \tag{10}$$

where the relations are schematically shown in Figure 2. Inserting equation (10) into equation (9), one has

$$\delta W(t) = -\sum_{i=1}^{N} [k_{i1}(v_S \delta v_S + w_S \delta w_S) + k_{i2}(w_S \delta v_S - v_S \delta w_S) + c_{i1}(\dot{v}_S \delta v_S + \dot{w}_S \delta w_S) + c_{i2}(\dot{w}_S \delta v_S - \dot{v}_S \delta w_S) - c_{i1}\Omega(w_S \delta v_S - v_S \delta w_S) + c_{i2}\Omega(v_S \delta v_S + w_S \delta w_S)]|_{bi}. \tag{11}$$

3.2. DISCRETIZATION OF THE DISTRIBUTED SYSTEM

As an approximate treatment, the displacements of the continuous shaft and disk substructures will be assumed in the form of a series composed of a linear combination of weighted admissible functions (assumed modes method). The eigenfunctions of the transverse vibration of a free–free flexure and shear beam [24] will be chosen as the admissible functions for the transverse deflections of the shaft due to bending and due to shearing, respectively. The eigenfunctions of the free vibration of the corresponding stationary disk will be chosen as the admissible functions for the disks [5, 25]. With this conception and the fact that only one-nodal diameter modes of the disk couple with the shaft bending modes, the transverse displacement of the ith disk can be written as

$$u_{Di} = \cos \theta \mathbf{\Phi}_{Di}(r)\mathbf{Q}_{\xi i}(t) + \sin \theta \mathbf{\Phi}_{Di}(r)\mathbf{Q}_{\eta i}(t), \tag{12}$$

where $\mathbf{\Phi}_{Di}(r)$ is the row vector consisting of the admissible functions of the disk, and $\mathbf{Q}_{\xi i}(t)$ and $\mathbf{Q}_{\eta i}(t)$ are column vectors consisting of the corresponding time-dependent generalized co-ordinates of the ith disk.

The shaft bending displacement will take the form

$$v_{S1} = \mathbf{\Phi}_{S1}(x)\mathbf{Q}_{V1}(t), \quad w_{S1} = \mathbf{\Phi}_{S1}(x)\mathbf{Q}_{W1}(t), \tag{13}$$

and

$$v_{S2} = \mathbf{\Phi}_{S2}(x)\mathbf{Q}_{V2}(t), \quad w_{S2} = \mathbf{\Phi}_{S2}(x)\mathbf{Q}_{W2}(t), \tag{14}$$

where $\mathbf{\Phi}_{S1}(x)$ and $\mathbf{\Phi}_{S2}(x)$ are the row vectors consisting of the admissible functions of the shaft which describe the shaft motions in two orthogonal planes caused by bending and shearing, respectively; and $\mathbf{Q}_{V1}(t)$ and $\mathbf{Q}_{W1}(t)$, and $\mathbf{Q}_{V2}(t)$

and $\mathbf{Q}_{W2}(t)$ are column vectors consisting of the corresponding time-dependent generalized co-ordinates.

Substituting equations (12)–(14) into equations (6)–(8) and (11), using matrix formulation, and reducing lead to the discretized total energy functions

$$T = T_s + T_D, \quad V = V_S + V_D, \quad \partial W = \sum_{k=1}^{N_0} R_k \, \delta q_k, \tag{15}$$

where the detailed expressions are summarized in Appendix B, and N_0 is the number of degrees of freedom of the total discretized system.

3.3. GOVERNING EQUATIONS

In the last section, the total kinetic and potential energies and the virtual work have been expressed in terms of a limited number of generalized co-ordinates. Then Lagrange's equations are the direct choice for the formulation of the ordinary differential equations of motion of the total structure. Lagrange's equations take the form

$$\frac{\mathrm{d}}{\mathrm{d}t}\left(\frac{\partial L}{\partial \dot{q}_k}\right) - \frac{\partial L}{\partial q_k} = R_k, \qquad k = 1, 2, \ldots, N_0, \tag{16}$$

where $L(= T - V)$, $q_k(\mathbf{Q}_{V1}, \mathbf{Q}_{W1}, \mathbf{Q}_{V2}, \mathbf{Q}_{W2}, \mathbf{Q}_{\xi i}$ and $\mathbf{Q}_{\eta i})$, and R_k are the Lagrangian, generalized co-ordinates, and the forces which are not included in the potential energy function, respectively. Introducing equation (15) into equation (16) leads to a coupled set of equations. The generalized complex co-ordinates are defined, with two orthogonal generalized co-ordinates being the real and imaginary parts of a complex co-ordinate, as

$$\mathbf{Z}_{S1} = \mathbf{Q}_{V1} + j\mathbf{Q}_{W1}, \quad \mathbf{Z}_{S2} = \mathbf{Q}_{V2} + j\mathbf{Q}_{W2}, \quad \mathbf{Z}_{Di} = \mathbf{Q}_{\xi i} + j\mathbf{Q}_{\eta i}.$$

Employing the complex co-ordinates, the coupled equations of motion are expressed in matrix notation as

$$\begin{bmatrix} \mathbf{M}_{S1} & \mathbf{M}_{S12} & -\mathbf{M}_{SD1} & \cdots & -\mathbf{M}_{SDM} \\ \mathbf{M}_{S12}^T & \mathbf{M}_{S2} & \mathbf{0} & \cdots & \mathbf{0} \\ -\mathbf{M}_{SD1}^T & \mathbf{0} & \mathbf{M}_{D1} & \mathbf{0} & \\ \vdots & \vdots & \mathbf{0} & \ddots & \\ -\mathbf{M}_{SDM}^T & \mathbf{0} & & & \mathbf{M}_{DM} \end{bmatrix} \begin{Bmatrix} \ddot{\mathbf{Z}}_{S1} \\ \ddot{\mathbf{Z}}_{S2} \\ \ddot{\mathbf{Z}}_{D1} \\ \vdots \\ \ddot{\mathbf{Z}}_{DM} \end{Bmatrix}$$

$$+ \begin{bmatrix} \mathbf{C}_{11} & \mathbf{C}_{12} & \mathbf{0} & \cdots & \mathbf{0} \\ \mathbf{C}_{12}^T & \mathbf{C}_{22} & \mathbf{0} & \cdots & \mathbf{0} \\ \mathbf{0} & \mathbf{0} & \mathbf{0} & \mathbf{0} & \\ \vdots & \vdots & \mathbf{0} & \ddots & \\ \mathbf{0} & \mathbf{0} & & & \mathbf{0} \end{bmatrix} \begin{Bmatrix} \dot{\mathbf{Z}}_{S1} \\ \dot{\mathbf{Z}}_{S2} \\ \dot{\mathbf{Z}}_{D1} \\ \vdots \\ \dot{\mathbf{Z}}_{DM} \end{Bmatrix}$$

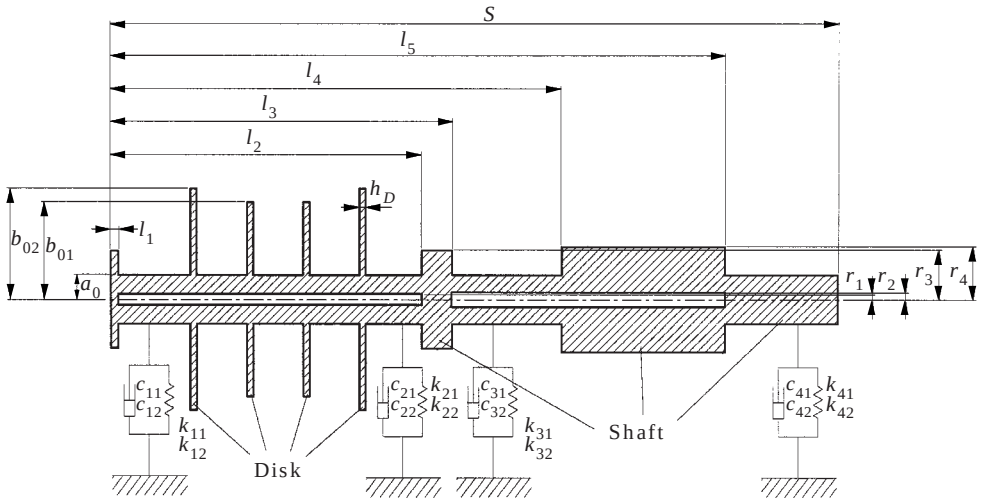

Figure 4. Cross-sectional view of the numerical model.

$$+\begin{bmatrix} \mathbf{K}_{11} & \mathbf{K}_{12} & -\Omega^2\mathbf{M}_{SD1} & \cdots & -\Omega^2\mathbf{M}_{SDM} \\ \mathbf{K}_{12}^T & \mathbf{K}_{22} & \mathbf{0} & \cdots & \mathbf{0} \\ -\Omega^2\mathbf{M}_{SD1}^T & \mathbf{0} & (\mathbf{K}_{D1}+\mathbf{K}_{D1}^T)/2 & \mathbf{0} & \\ \vdots & \vdots & \mathbf{0} & \ddots & \\ -\Omega^2\mathbf{M}_{SDM}^T & \mathbf{0} & & & (\mathbf{K}_{DM}+\mathbf{K}_{DM}^T)/2 \end{bmatrix} \begin{Bmatrix} \mathbf{Z}_{S1} \\ \mathbf{Z}_{S2} \\ \mathbf{Z}_{D1} \\ \vdots \\ \mathbf{Z}_{DM} \end{Bmatrix} = \begin{Bmatrix} \mathbf{0} \\ \mathbf{0} \\ \mathbf{0} \\ \vdots \\ \mathbf{0} \end{Bmatrix}, \tag{17}$$

where

$$\mathbf{C}_{11} \equiv \overset{(3)}{\mathbf{K}}{}_{S1}^{(3)} + j[\Omega(\mathbf{K}_{S1}^{(1)} + \mathbf{M}_{S1}) - \overset{(4)}{\mathbf{K}}{}_{S1}^{(3)}],\ \mathbf{C}_{12} \equiv \overset{(3)}{\mathbf{K}}{}_{S12}^{(3)} + j(2\Omega\mathbf{M}_{S12} - \overset{(4)}{\mathbf{K}}{}_{S12}^{(3)}),$$

$$\mathbf{C}_{22} \equiv \overset{(3)}{\mathbf{K}}{}_{S2}^{(3)} + j[2\Omega\mathbf{M}_{S2} - \overset{(4)}{\mathbf{K}}{}_{S2}^{(3)}],$$

$$\mathbf{K}_{11} \equiv -\Omega^2\mathbf{K}_{S1}^{(1)} + \mathbf{K}_{S1}^{(2)} + \overset{(1)}{\mathbf{K}}{}_{S1}^{(3)} - j\overset{(2)}{\mathbf{K}}{}_{S1}^{(3)},\ \mathbf{K}_{12} \equiv -\Omega^2\mathbf{M}_{S12} + \overset{(1)}{\mathbf{K}}{}_{S12}^{(3)} - j\overset{(2)}{\mathbf{K}}{}_{S12}^{(3)},$$

$$\mathbf{K}_{22} \equiv -\Omega^2\mathbf{M}_{S2} + \mathbf{K}_{S2}^{(2)} + \overset{(1)}{\mathbf{K}}{}_{S2}^{(3)} - j\overset{(2)}{\mathbf{K}}{}_{S2}^{(3)},$$

and the element matrices are given in Appendix C.

4. NUMERICAL SIMULATION

To illustrate the efficiency of the present method, a rotor model of typical dimensions for the utility industry (turbine-generator set) is studied. The model shown in Figure 4 consists of a long shaft, four uniform disks, and four journal bearings. The details of the system configuration (Figures 1 and 4) are listed as follows (in mm): $a_0 = 380$, $b_{01} = 1750$, $b_{02} = 1550$, $r_1 = 75$, $r_2 = 115$, $r_3 = 769$,

$r_4 = 824$, $b_1 = 1203$, $b_2 = 9281$, $b_3 = 12\,151$, $b_4 = 21\,809$, $d_1 = 2613$, $d_2 = 4399$, $d_3 = 6185$, $d_4 = 7971$, $h_D = 200$, $l_1 = 230$, $l_2 = 10\,126$, $l_3 = 11\,106$, $l_4 = 14\,844$, $l_5 = 20\,026$, and $S = 23\,599$. The material and bearing properties are: $\rho = 7700\,\text{kg/m}^3$, $E = 19{\cdot}0 \times 10^{10}\,\text{N/m}^2$, $\nu = 0{\cdot}3$, $k_{11} = k_{21} = 2{\cdot}0 \times 10^9\,\text{N/m}$, $k_{31} = k_{41} = 3{\cdot}0 \times 10^9\,\text{N/m}$, $k_{12} = k_{22} = k_{32} = k_{42} = 0{\cdot}0\,\text{N/m}$, $c_{11} = c_{21} = c_{31} = c_{41} = 6{\cdot}5 \times 10^5\,\text{N s/m}$, and $c_{12} = c_{22} = c_{32} = c_{42} = 0{\cdot}0\,\text{N s/m}$.

4.1. ADMISSIBLE FUNCTIONS

According to the substructure synthesis, the displacements of the continuous shaft and disks are assumed in the form of a series composed of a weighted linear summation of admissible functions, as shown in equations (12)–(l4). Mode shapes of the non-rotating uniform beam with free–free boundary conditions and the non-rotating uniform circular plate with inner clamped–outer free boundary conditions are used as the admissible functions for the shaft and the disks, respectively. The formulas used to obtain the admissible functions are as follows.

The flexural (bending) deflections of a slender free–free shaft ($0 \leqslant x/S \leqslant 1{\cdot}0$, S is the length of the shaft), with rotary inertia ignored:

$$Y_1(x) = 1{\cdot}0, \quad Y_2(x) = \sqrt{12}(x/S - 0{\cdot}5),$$
$$Y_i(x) = \cosh(\lambda_i x/S) + \cos(\lambda_i x/S) - \sigma_i[\sinh(\lambda_i x/S) + \sin(\lambda_i x/S)], \quad i = 3, 4, 5, \ldots,$$
$$\sigma_i = (\cosh\lambda_i - \cos\lambda_i)/(\sinh\lambda_i - \sin\lambda_i).$$

The transcendental equation for the dimensionless natural frequency parameter λ is

$$\cos\lambda \cosh\lambda = 1.$$

The shearing deflections of a free–free shaft are

$$Y_i(x) = \sqrt{2}\cos(i\pi x/S), \qquad i = 1, 2, 3, \ldots.$$

The transverse deflections of the disks are

$$R_{1n}(r) = A_N J_1(\beta_n r/b_{0i}) + B_n Y_1(\beta_n r/b_{0i} + C_n I_1(\beta_n r/b_{0i}) + D_n K_1(\beta_n r/b_{0i}),$$
$$n = 0, 1, 2, \ldots, \; i = 1, 2,$$

where subscript "1" designates the modes of one nodal diameter, and n is the number of the nodal circles, not counting the nodal circle enforced by the inner clamped boundary condition; J_1 and Y_1 are Bessel functions of the first and second kind, respectively, and I_1 and K_1 are the modified Bessel functions of the first and second kind, respectively; A_n, B_n, C_n, and D_n are constants determined by the boundary conditions, nodal circle number and the normalized condition; β_n is a dimensionless parameter, and β_n is related to the natural frequency ω_n (rad/s) by

$$\beta_n^4 = \omega_n^2 \frac{\rho_D h_D b_0^4}{D},$$

where the β_n are determined by setting the coefficient determinant of the linear equation set, derived by the boundary conditions, to zero [5, 25].

Some lowest mode shapes for the admissible functions are depicted in Figure 5, where the natural frequencies of the disk modes are also listed.

4.2. CONVERGENCE

A convergence study is carried out, as shown in Tables 1–3, where the bold terms are those unchanged compared with the previous calculation. DOF stands for the degree of freedom of the total discretized system, NS1 is the number of admissible functions for the bending deflections of the shaft, NS2 is the number of admissible functions for the shearing deflections of the shaft, and ND is the number of admissible functions for the transverse deflections of the disks. From Table 1, one sees that when NS1 = 26, satisfactory convergence is attained for the value precision used here. For NS2 and ND, the convergence is relatively much more rapid. This is because the contribution from the shearing deformation is much smaller than that from the bending deformation, and the

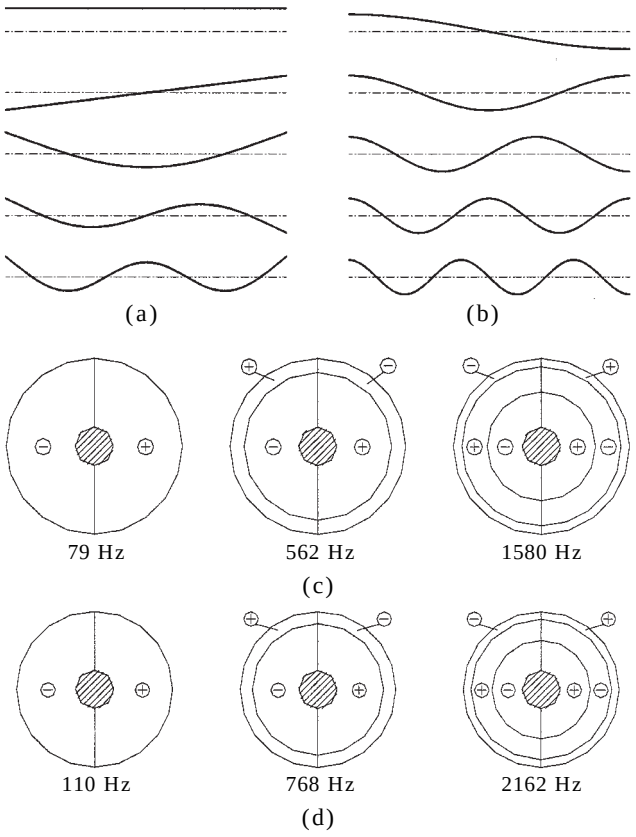

Figure 5. Some lowest admissible functions for (a) the bending deflections of the shaft, (b) the shearing deflections of the shaft, (c) the transverse deflections of the disks of radius 1750 mm, and (d) the transverse deflections of the disks of radius 1550 mm.

TABLE 1

Convergence study: admissible functions for the bending deflections of the shaft (NS1)

DOF	NS1	NS2	ND	ω_1	ω_2	ω_3	ω_4	ω_5	ω_6	ω_7	ω_8	ω_9	ω_{10}	ω_{11}	ω_{12}	ω_{13}	ω_{14}	ω_{15}
56	10	**10**	**2**	16·0	25·9	40·9	52·5	60·0	67·4	84·2	87·3	94·5	111·4	121·2	142·6	235·8	349·8	563·6
66	15	**10**	**2**	15·3	23·9	39·9	52·1	59·2	64·2	67·9	76·8	80·3	102·9	115·3	135·2	177·3	224·3	295·0
76	20	**10**	**2**	15·2	23·3	39·7	52·0	58·5	63·3	67·7	76·6	79·9	101·6	114·6	131·0	169·8	189·2	270·6
80	22	**10**	**2**	**15·2**	23·0	39·6	51·8	**58·5**	**63·3**	**67·7**	76·3	**79·9**	100·3	112·8	128·0	168·0	188·2	268·0
84	24	**10**	**2**	15·1	**23·0**	**39·6**	51·7	**58·5**	63·2	**67·7**	76·1	79·6	97·9	111·8	127·5	167·5	187·3	262·4
88	26	**10**	**2**	**15·1**	**23·0**	**39·6**	**51·7**	58·4	**63·2**	67·6	**76·1**	**79·6**	97·5	111·3	**127·5**	167·4	187·2	262·3

TABLE 2

Convergence study: admissible functions for the shearing deflections of the shaft (*NS*2)

DOF	NS1	NS2	ND	ω_1	ω_2	ω_3	ω_4	ω_5	ω_6	ω_7	ω_8	ω_9	ω_{10}	ω_{11}	ω_{12}	ω_{13}	ω_{14}	ω_{15}
68	**26**	0	**2**	15·102	22·990	39·575	51·711	58·445	63·205	67·627	76·109	79·642	97·490	111·32	127·48	167·41	187·24	262·32
78	**26**	5	**2**	**15·102**	22·989	**39·575**	**51·711**	**58·445**	**63·205**	**67·627**	**76·109**	**79·641**	97·485	**111·32**	**127·48**	167·40	187·23	262·32
88	**26**	10	**2**	**15·102**	**22·989**	39·574	**51·711**	58·444	63·204	67·625	76·108	**79·641**	97·483	**111·32**	127·47	167·39	187·22	262·29
98	**26**	15	**2**	**15·102**	22·988	**39·574**	**51·711**	**58·444**	**63·204**	**67·625**	**76·108**	**79·641**	**97·483**	**111·32**	**127·47**	**167·39**	187·21	262·27

TABLE 3

Convergence study: admissible functions for the transverse deflections of the disks (ND)

DOF	NS1	NS2	ND	ω_1	ω_2	ω_3	ω_4	ω_5	ω_6	ω_7	ω_8	ω_9	ω_{10}	ω_{11}	ω_{12}	ω_{13}	ω_{14}	ω_{15}
72	**26**	**10**	0	15·114	22·990	39·777	53·048	58·866	66·937	70·302	98·743	128·68	157·05	183·51	265·38	322·72	350·82	375·18
80	**26**	**10**	1	15·102	22·989	39·574	51·711	58·445	63·205	67·625	76·108	79·642	97·485	111·32	127·48	167·46	187·30	262·51
88	**26**	**10**	2	**15·102**	**22·989**	**39·574**	51·711	**58·444**	63·204	**67·625**	**76·108**	79·641	97·483	**111·32**	127·47	167·39	187·22	262·29
112	**26**	**10**	**5**	**15·102**	**22·989**	**39·574**	**51·711**	**58·444**	**63·204**	**67·625**	**76·108**	**79·641**	**97·483**	**111·32**	**127·47**	**167·39**	**187·22**	262·28

natural frequencies of the higher disk modes are much larger than the frequency range considered in the discussion. From the convergence study, one chooses NS1 = 26, NS2 = 10, and ND = 2 to describe the local deflections of each element, and a total of 88 degrees of freedom are obtained for the discretized system (26×2 for the shaft two-degree-of-freedom bending defections, 10×2 for the shaft two-degree-of freedom shearing defections, and $(2 \times 2) \times 4$ for the two-degree-of-freedom transverse deflections of four disks).

5. RESULTS AND DISCUSSION

5.1. BENDING COUPLED NATURAL FREQUENCIES

The equations of motion (17) were derived in the rotating co-ordinate system X_1–Y_1–Z_1 for the shaft and X_2–Y_2–Z_2 for the disks. Then the natural frequencies were obtained in the rotating co-ordinates. For comparing with experimental results, which are generally obtained relative to a stationary observer, it is necessary to show the natural frequencies in stationary co-ordinates. Since the transformation relations from the rotating co-ordinates to the stationary co-ordinates are different in view of the shaft transverse vibration and in view of the disk transverse vibration, there will be two sets of different natural frequencies in stationary co-ordinates.

In view of the shaft transverse vibration, the relation is

$$\omega_0 = \omega + \Omega, \tag{18}$$

where ω is the natural frequency in rotating co-ordinates including both positive values for forward modes and negative values for backward modes, Ω is the shaft rotating speed and ω_0 is the natural frequency in stationary co-ordinates.

In view of the disk transverse vibration, the transformation from rotating co-ordinates (X_2–Y_2–Z_2 system, which is fixed in the disk) to stationary co-ordinates (X_0–Y_0–Z_0 system, which is stationary in the space) (see Figure 2) is not without some difficulty. Compared to the rotation angle Ωt, the small vibration angles θ_ξ and θ_η may be ignored for the purpose of co-ordinate transformation. Then the angular co-ordinates of the two systems are connected by the relation

$$\theta_0 = \theta + \Omega t.$$

The response of the disk to a stationary force ($F_0 \cos \omega_0 t$, acting at $r_0 = \rho$, and $\theta_0 = 0$) in space is [26]

$$u = K(\rho, m) F_0 f(r) \cos m\theta \left[\frac{\cos(\omega_0 + m\Omega)t}{|\omega^2 - (\omega_0 + m\Omega)^2|} + \frac{\cos(\omega_0 - m\Omega)t}{|\omega^2 - (\omega_0 - m\Omega)^2|} \right], \tag{19}$$

where ω is the natural frequency in rotating co-ordinates, m is the nodal diameter number of the disk mode. From formula (19), it is seen that there are two resonant frequencies relative to a stationary observer:

$$\omega_0 = \omega + m\Omega, \quad \text{and} \quad \omega_0 = \begin{cases} \omega - m\Omega & \text{for } \omega \geqslant m\Omega, \\ -(\omega - m\Omega) & \text{for } \omega < m\Omega. \end{cases} \tag{20}$$

Note that the natural frequency value of the disk transverse vibration should be positive. $\omega - m\Omega$ and $-(\omega - m\Omega)$ is a continuous curve when drawn as a frequency–speed diagram, so one generally states that every natural frequency splits into two branches when rotating. This is saying that two excitation frequencies stationary in space will excite the same resonant mode at a given angular velocity, which has been well verified by experimental results [16].

For the specific problem discussed in the paper, ω is the coupled shaft–disk natural frequency, which can be negative in value resulted from the backward precessional modes of the rotor system; and $m = 1$ since only modes of one nodal diameter contribute to the bending coupled vibration. The transformation relation (20) will change to

$$\omega_0 = |\omega| + \Omega, \quad \text{and} \quad \omega_0 = \begin{cases} |\omega| - \Omega & \text{for } |\omega| \geqslant \Omega, \\ -(|\omega| - \Omega) & \text{for } |\omega| < \Omega. \end{cases} \tag{21}$$

According to formula (18), the coupled natural frequencies, in view of the shaft transverse vibration, are shown in Figures 6(a) and (b) for the flexible-shaft/rigid-disk model and the flexible-shaft/flexible-disk model, respectively. According to formula (21), the coupled natural frequencies for the flexible-shaft/flexible-disk model, in view of the disk transverse vibration, are shown in Figures 7(a) and (b) for the forward precessional modes and the backward precessional modes, respectively. Note that, for the flexible-shaft/rigid-disk model, the natural frequencies in view of disk transverse vibration are the same as those in view of the shaft transverse vibration.

5.2. BENDING COUPLED MODE SHAPES

The ten lowest coupled mode shapes and the corresponding frequency values, at zero rotating speed, are shown in Figure 8(a) without considering disk flexibility and Figure 8(b) considering disk flexibility. One sees that for modes (1) and (2) in Figure 8(a), and modes (1) and (2) in Figure 8(b), the disk flexibility does not have visible influence on both the natural frequency values and the mode shapes within the precision shown. For the comparable modes (3)–(6), the disk flexibility reduces the natural frequency values, and has some influence on the mode shapes. Modes (1)–(6) are called shaft-dominating modes, which can be well predicted without considering disk flexibility and the inclusion of disk flexibility will reduce or have negligible influence on the natural frequency values. Other modes in Figure 8(a) do not have comparable partners in Figure 8(b). One notes that the natural frequencies of these modes are around the natural frequencies (79 and 110 Hz) of the first disk modes shown in Figures 5(c) and (d). For modes (7), (8) and (10) in Figure 8(b), the shaft has obvious deflections at the disk locations, and the disks deform in such a manner that their inertia moments on the shaft do not cancel out. These modes are called

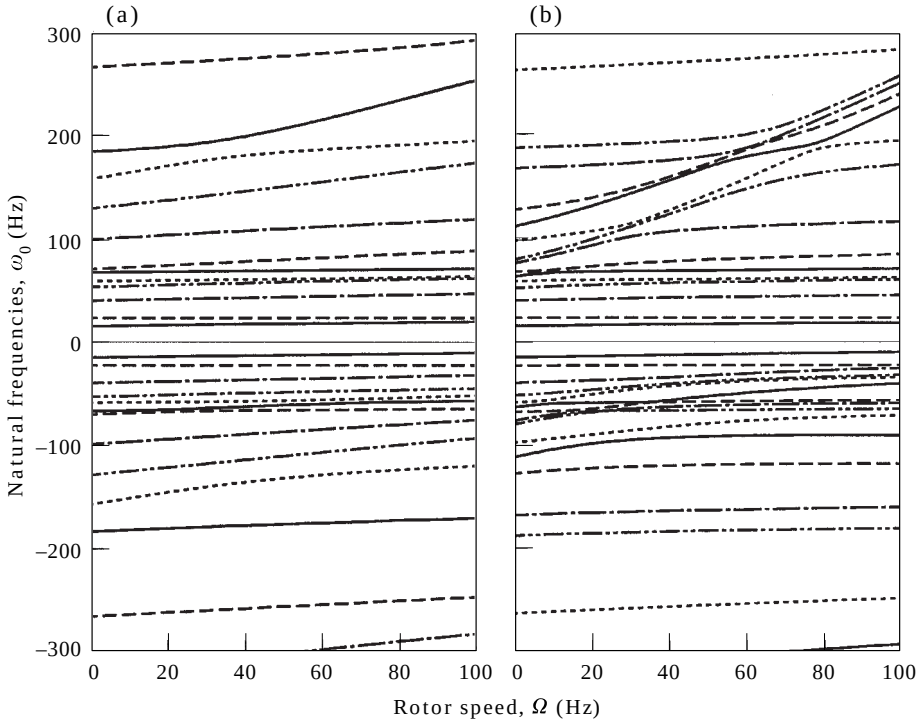

Figure 6. Coupled modal frequencies of the rotor system in view of the shaft transverse vibration. (a) Flexible shaft and rigid disks, and (b) flexible shaft and flexible disks. Key for (a): 12 forward and 13 backward natural frequencies are drawn within the range of (−300 Hz, 300 Hz); key for (b): 15 forward and 16 backward natural frequencies are drawn within the range of (−300 Hz, 300 Hz).

shaft–disk coupled modes. They cannot be predicted without considering disk flexibility or shaft flexibility. For mode (9) in Figure 8(b), the shaft has small deflections, especially at the disk locations, and the disks deform in such a manner that their inertia moments on the shaft cancel out. These modes are called disk-dominating modes. They cannot be predicted without considering disk flexibility and can be well predicted without considering shaft flexibility (first mode of the larger disks). The calculation without considering shaft flexibility is out of the scope of this paper and will be discussed in further research output. Now returning to the natural frequencies in Figure 6. For the shaft-dominating mode, good comparability is attained between Figures 6(a) and (b). Due to the introduction of shaft–disk coupled modes and disk-dominating modes around the natural frequency of the first disk modes, the natural frequencies in Figure 6(b) become complicated between around 70 and 160 Hz and are difficult to compare with Figure 6(a), especially at low spinning speeds. Some of these natural frequencies increase rapidly as the rotor speed increases, which is caused by the centrifugal stiffening as a result of rotation of the flexible disks. The centrifugal stiffening effect is introduced through disk potential energy as the term

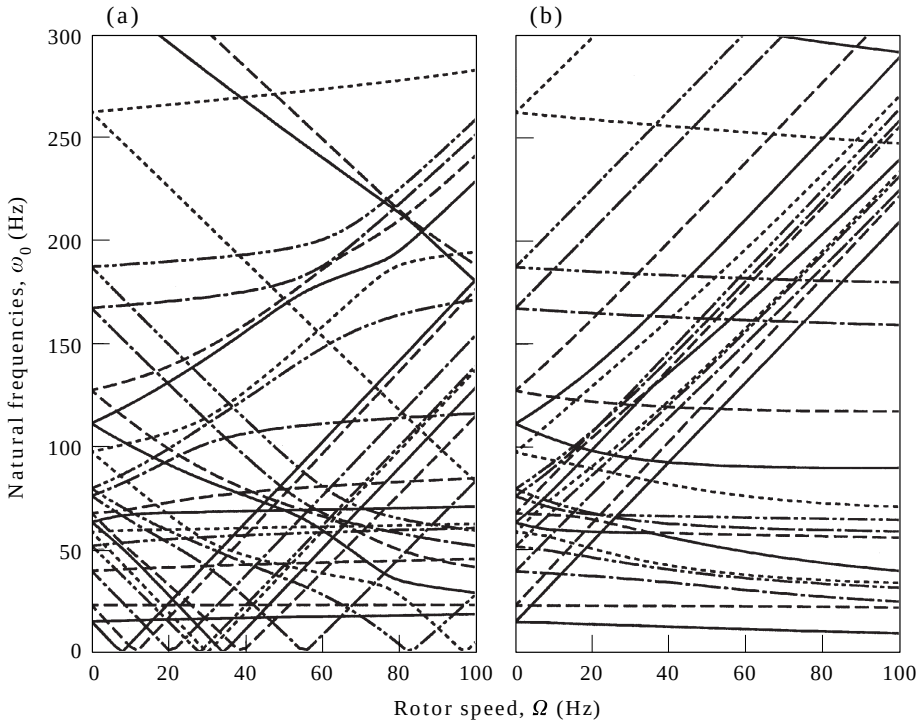

Figure 7. Coupled modal frequencies of the rotor system in view of the disk transverse vibration. (a) Forward precessional modes, and (b) backward precessional modes. Key for (a): 17 forward natural frequencies are drawn within the range of (0 Hz, 300 Hz); key for (b): 16 backward natural frequencies are drawn within the range of (0 Hz, 300 Hz).

$$\frac{1}{2}\int_0^{2\pi}\int_{a_{0i}}^{b_{0i}}\left[N_r\left(\frac{\partial u_{Di}}{\partial r}\right)^2+N_\theta\left(\frac{1}{r}\frac{\partial u_{Di}}{\partial \theta}\right)^2\right]r\,\mathrm{d}r\,\mathrm{d}\theta.$$

At high rotational speeds, good comparability appears between Figures 6(a) and (b) for the modes around 70–160 Hz since the disks become stiffer due to rotation.

For the higher natural frequencies above 180 Hz, the shaft-dominating modes appear again due to the far separation from the disk natural frequencies. These modes will not be discussed in detail here since they are far from the frequency range of practical concern.

6. SUMMARY AND CONCLUSIONS

The intricate coupled vibration problem of a spinning Timoshenko beam/disk/bearing system was investigated based on the flexible-shaft/flexible-disk model. According to the nature of coupling with the shaft, disk vibratory modes are classified into three groups: uncoupled disk modes with more than one nodal diameter, disk modes with a single nodal diameter coupled with the shaft bending vibrations and axisymmetric modes coupled with the shaft

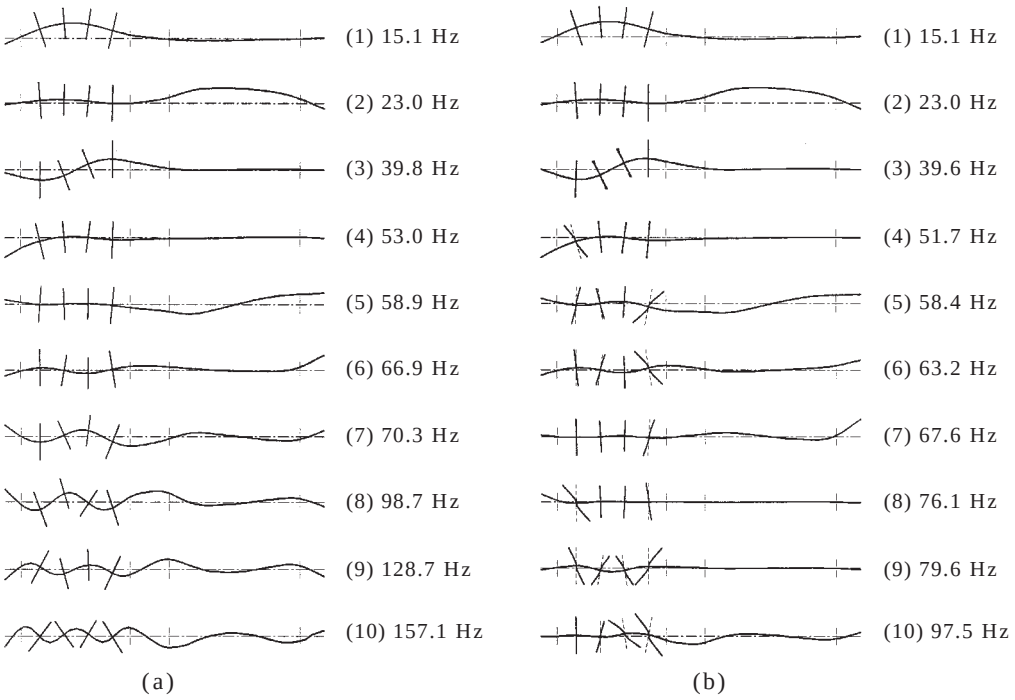

Figure 8. Coupled vibration mode shapes of (a) the flexible-shaft/rigid-disk model, and (b) the flexible-shaft/flexible-disk model ($\Omega = 0$ rpm).

longitudinal(axial) vibrations. The bending coupled vibrations of single nodal diameter disk modes and the shaft-bearing system were solved by a substructure synthesis technique. The centrifugal stiffening effect of disks was included in the formulation. The coupled natural frequencies, both in view of the shaft transverse vibration and in view of the disk transverse vibration, and the coupled mode shapes at stationary state were obtained for an idealized turbine-generator set. For the typical rotor case examined, the disk flexibility will have important influence on the vibration characteristics of the rotor system, especially at the natural frequency range around the disk natural frequencies. By including disk flexibility, the coupled modes of the shaft/disk/bearing system may be divided into three types: the shaft-dominating modes, the shaft–disk coupled modes, and the disk-dominating modes. Disk flexibility will reduce the natural frequency values of some shaft-dominating modes and has negligible influence on others. The shaft–disk coupled modes, and the disk-dominating modes cannot be predicted without considering disk flexibility.

As a rule of thumb, disk flexibility can be ignored if the frequency range of interest is far from the disk natural frequencies, otherwise the coupled flexible-shaft/flexible-disk analysis must be performed.

REFERENCES

1. G. R. KIRCHHOFF 1850 *Crelle's Journal (Jour. Math.)* **40**, 51–88. Über das Gleichgewicht und die Bewegung einer elastischen Scheibe.

2. G. R. KIRCHHOFF 1850 *Poggendorff's Annal* **81**, 258–264. Über die Schwingungen einer Kreisförmigen elastischen Scheibe.
3. LORD RAYLEIGH 1945 *The Theory of Sound* (two volumes). New York: Dover Publications; second edition. See Volume 1, pp. 352–394.
4. H. LAMB and R. V. SOUTHWELL 1921 *Proceedings of the Royal Society, London, Series A* **99**, 272–280. The vibration of a spinning disk.
5. R. V. SOUTHWELL 1922 *Proceedings of the Royal Society, London, Series A* **101**, 133–152. On the free transverse vibrations of a uniform circular disc clamped at its center; and on the effects of rotation.
6. C. D. MOTE, JR. 1970 *Journal of the Franklin Institute* **290**, 329–344. Stability of circular plates subjected to moving loads.
7. H. S. JIA, S. B. CHUN and C. W. LEE 1997 *Journal of Sound and Vibration* **208**, 175–187. Evaluation of the longitudinal coupled vibrations in rotating, flexible disks/spindle systems.
8. J. A. DOPKIN and T. E. SHOUP 1974 *American Society of Mechanical Engineers Journal of Engineering for Industry* **96**, 1328–1333. Rotor resonant speed reduction caused by flexibility of disks.
9. D. R. CHIVENS and H. D. NELSON 1975 *American Society of Mechanical Engineers Journal of Engineering for Industry* **97**, 881–886. The natural frequencies and critical speeds of a rotating, flexible shaft–disk system.
10. F. J. WILGEN and A. L. SCHLACK 1979 *American Society of Mechanical Engineers Journal of Mechanical Design* **101**, 298–303. Effects of disk flexibility on shaft whirl stability.
11. A. A. S. SHAHAB and J. THOMAS 1987 *Journal of Sound and Vibration* **114**, 435–452. Coupling effects of disc flexibility on the dynamic behavior of multi disc–shaft systems.
12. J. M. VANCE 1988 *Rotordynamics of Turbomachinery*. New York: Wiley. See pp. 137–169.
13. F. WU and G. T. FLOWERS 1992 *American Society of Mechanical Engineers Journal of Vibration and Acoustics* **114**, 242–248. A transfer matrix technique for evaluating the natural frequencies and critical speeds of a rotor with multiple flexible disks.
14. I. Y. SHEN and C.-P. R. KU 1997 *American Society of Mechanical Engineers Journal of Applied Mechanics* **64**, 165–174. A nonclassical vibration analysis of a multiple rotating disk and spindle assembly.
15. L. MEIROVITCH 1980 *Computational Methods in Structural Dynamics*. The Netherlands: Sijthoff & Noordhoff. See pp. 298–300 and 401–409.
16. C. W. LEE, H. S. JIA, C. S. KIM and S. B. CHUN 1997 *Journal of Sound and Vibration* **207**, 435–451. Tuning of simulated natural frequencies for a flexible shaft-multiple flexible disk system.
17. LORD RAYLEIGH 1945 *The Theory of Sound* (two volumes). New York: Dover Publications; second edition. See Volume 1, pp. 255–294.
18. S. P. TIMOSHENKO 1921 *Philosophical Magazine* **41**, 744–746. On the correction for shear of the differential equation for transverse vibrations of prismatic bars.
19. S. P. TIMOSHENKO 1922 *Philosophical Magazine* **43**, 125–131. On the transverse vibrations of bars of uniform cross-section.
20. H. S. JIA and C. W. LEE 1998 *KSME International Journal* **12**, 223–232. On the vibration of imperfect circular disks.
21. L. MEIROVITCH 1967 *Analytical Methods in Vibrations*. New York: Macmillan. See pp. 179–189.
22. W.-R. CHEN and L. M. KEER 1993 *American Society of Mechanical Engineers Journal of Vibration and Acoustics* **115**, 285–294. Transverse vibrations of a rotating twisted Timoshenko beam under axial loading.

23. C. W. Lee and S. B. Chun 1998 *American Society of Mechanical Engineers Journal of Vibration and Acoustics* **120**, 87–94. Vibration analysis of a rotor with multiple flexible disks using assumed modes method.
24. R. D. Blevins 1979 *Formulas for Natural Frequency and Mode Shape*. New York: Von Nostrand Reinhold. See pp. 101–182.
25. S. M. Vogl and D. W. Skinner 1965 *American Society of Mechanical Engineers Journal of Applied Mechanics* **32**, 926–931. Natural frequencies of transversely vibrating uniform annular plates.
26. S. A. Tobias and R. N. Arnold 1957 *Proceedings of the Institution of Mechanical Engineers* **171**, 669–690. The influence of dynamical imperfection on the vibration of rotating disks.

APPENDIX A: STRESSES, LAPLACIAN, AND FLEXURAL RIGIDITY

$$N_r = \frac{\rho_D h_D \Omega^2}{8}\left[-(3+v_D)r^2 + C_1 + C_2\frac{1}{r^2}\right],$$

$$N_\theta = \frac{\rho_D h_D \Omega^2}{8}\left[-(1+3v_D)r^2 + C_1 - C_2\frac{1}{r^2}\right],$$

$$C_1 = \frac{(1+v_D)(3+v_D)b^4 + (1-v_D^2)a^4}{(1+v_D)b^2 + (1-v_D)a^2}, C_2 = b^2a^2\frac{(1-v_D)(3+v_D)b^2 - (1-v_D^2)a^2}{(1+v_D)b^2 + (1-v_D)a^2},$$

$$\nabla^2 = \frac{\partial^2}{\partial r^2} + \frac{\partial}{r\partial r} + \frac{\partial^2}{r^2\,\partial\theta^2},\ D = \frac{E_D h_D^3}{12(1-v_D^2)}.$$

APPENDIX B: DISCRETIZED TOTAL ENERGY FUNCTIONS

$$\begin{aligned}
T &= T_S + T_D \\
&= \frac{1}{2}\dot{\mathbf{Q}}_{V1}^T\mathbf{M}_{S1}\dot{\mathbf{Q}}_{V1} + \frac{1}{2}\dot{\mathbf{Q}}_{W1}^T\mathbf{M}_{S1}\dot{\mathbf{Q}}_{W1} + \frac{1}{2}\dot{\mathbf{Q}}_{V2}^T\mathbf{M}_{S2}\dot{\mathbf{Q}}_{V2} + \frac{1}{2}\dot{\mathbf{Q}}_{W2}^T\mathbf{M}_{S2}\dot{\mathbf{Q}}_{W2} \\
&\quad + \dot{\mathbf{Q}}_{V1}^T\mathbf{M}_{S12}\dot{\mathbf{Q}}_{V2} + \dot{\mathbf{Q}}_{W1}^T\mathbf{M}_{S12}\dot{\mathbf{Q}}_{W2} \\
&\quad + \frac{1}{2}\Omega^2\mathbf{Q}_{V1}^T\mathbf{K}_{S1}^{(1)}\mathbf{Q}_{V1} + \frac{1}{2}\Omega^2\mathbf{Q}_{W1}^T\mathbf{K}_{S1}^{(1)}\mathbf{Q}_{W1} + \frac{1}{2}\Omega^2\mathbf{Q}_{V2}^T\mathbf{M}_{S2}\mathbf{Q}_{V2} + \frac{1}{2}\Omega^2\mathbf{Q}_{W2}^T\mathbf{K}_{S2}^{(1)}\mathbf{Q}_{W2} \\
&\quad + \Omega^2\mathbf{Q}_{V1}^T\mathbf{M}_{S12}\mathbf{Q}_{V2} + \Omega^2\mathbf{Q}_{W1}^T\mathbf{M}_{S12}\mathbf{Q}_{W2} \\
&\quad + \Omega\dot{\mathbf{Q}}_{W1}^T\mathbf{K}_{S1}^{(1)}\mathbf{Q}_{V1} - \Omega\dot{\mathbf{Q}}_{V1}^T\mathbf{M}_{S1}\mathbf{Q}_{W1} + \Omega\dot{\mathbf{Q}}_{W1}^T\mathbf{M}_{S12}\mathbf{Q}_{V2} - \Omega\dot{\mathbf{Q}}_{V1}^T\mathbf{M}_{S12}\mathbf{Q}_{W2} \\
&\quad + \Omega\mathbf{Q}_{V1}^T\mathbf{M}_{S12}\dot{\mathbf{Q}}_{W2} - \Omega\mathbf{Q}_{W1}^T\mathbf{M}_{S12}\dot{\mathbf{Q}}_{V2} + \Omega\dot{\mathbf{Q}}_{W2}^T\mathbf{M}_{S2}\mathbf{Q}_{V2} - \Omega\dot{\mathbf{Q}}_{V2}^T\mathbf{M}_{S2}\mathbf{Q}_{W2} \\
&\quad + \sum_{i=1}^{M}\frac{1}{2}(\dot{\mathbf{Q}}_{\xi i}^T\mathbf{M}_{Di}\dot{\mathbf{Q}}_{\xi i} + \dot{\mathbf{Q}}_{\eta i}^T\mathbf{M}_{Di}\dot{\mathbf{Q}}_{\eta i})
\end{aligned}$$

$$+\sum_{i=1}^{M}(-\dot{\mathbf{Q}}_{W1}^{T}\mathbf{M}_{SDi}\dot{\mathbf{Q}}_{\eta i}-\Omega\mathbf{Q}_{V1}^{T}\mathbf{M}_{SDi}\dot{\mathbf{Q}}_{\eta i}-\dot{\mathbf{Q}}_{V1}^{T}\mathbf{M}_{SDi}\dot{\mathbf{Q}}_{\xi i}+\Omega\mathbf{Q}_{W1}^{T}\mathbf{M}_{SDi}\dot{\mathbf{Q}}_{\xi i})$$

$$+\sum_{i=1}^{M}(-\Omega\dot{\mathbf{Q}}_{V1}^{T}\mathbf{M}_{SDi}\dot{\mathbf{Q}}_{\eta i}+\Omega^{2}\mathbf{Q}_{W1}^{T}\mathbf{M}_{SDi}\dot{\mathbf{Q}}_{\eta i}+\Omega\dot{\mathbf{Q}}_{W1}^{T}\mathbf{M}_{SDi}\mathbf{Q}_{\xi i}+\Omega^{2}\mathbf{Q}_{V1}^{T}\mathbf{M}_{SDi}\mathbf{Q}_{\xi i}),$$

$$V=V_S+V_D$$
$$+\sum_{i=1}^{M}\frac{1}{2}(\mathbf{Q}_{\xi i}^{T}\mathbf{K}_{Di}\mathbf{Q}_{\xi i}+\mathbf{Q}_{\eta i}^{T}\mathbf{K}_{Di}\mathbf{Q}_{\eta i})+\frac{1}{2}\mathbf{Q}_{V1}^{T}\mathbf{K}_{S1}^{(2)}\mathbf{Q}_{V1}+\frac{1}{2}\mathbf{Q}_{W1}^{T}\mathbf{K}_{S1}^{(2)}\mathbf{Q}_{W1}$$
$$+\frac{1}{2}\mathbf{Q}_{V2}^{T}\mathbf{K}_{S2}^{(2)}\mathbf{Q}_{V2}+\frac{1}{2}\mathbf{Q}_{W2}^{T}\mathbf{K}_{S2}^{(2)}\mathbf{Q}_{W2},$$

$$\begin{aligned}\delta W(t)=&-\Big(\mathbf{Q}_{V1}^{T}\overset{(1)}{\mathbf{K}}{}_{S1}^{(3)}+\mathbf{Q}_{V2}^{T}\overset{(1)}{\mathbf{K}}{}_{S12}^{(3)T}+\mathbf{Q}_{W1}^{T}\overset{(2)}{\mathbf{K}}{}_{S1}^{(3)}+\mathbf{Q}_{W2}^{T}\overset{(2)}{\mathbf{K}}{}_{S12}^{(3)T}+\dot{\mathbf{Q}}_{V1}^{T}\overset{(3)}{\mathbf{K}}{}_{S1}^{(3)}+\dot{\mathbf{Q}}_{V2}^{T}\overset{(3)}{\mathbf{K}}{}_{S12}^{(3)T}\\&+\dot{\mathbf{Q}}_{W1}^{T}\overset{(4)}{\mathbf{K}}{}_{S1}^{(3)}+\dot{\mathbf{Q}}_{W2}^{T}\overset{(4)}{\mathbf{K}}{}_{S12}^{(3)T}\Big)\delta\mathbf{Q}_{V1}\\&-\Big(\mathbf{Q}_{W1}^{T}\overset{(1)}{\mathbf{K}}{}_{S1}^{(3)}+\mathbf{Q}_{W2}^{T}\overset{(1)}{\mathbf{K}}{}_{S12}^{(3)T}-\mathbf{Q}_{V1}^{T}\overset{(2)}{\mathbf{K}}{}_{S1}^{(3)}-\mathbf{Q}_{V2}^{T}\overset{(2)}{\mathbf{K}}{}_{S12}^{(3)T}+\dot{\mathbf{Q}}_{W1}^{T}\overset{(3)}{\mathbf{K}}{}_{S1}^{(3)}+\dot{\mathbf{Q}}_{W2}^{T}\overset{(3)}{\mathbf{K}}{}_{S12}^{(3)T}\\&-\dot{\mathbf{Q}}_{V1}^{T}\overset{(4)}{\mathbf{K}}{}_{S1}^{(3)}-\dot{\mathbf{Q}}_{V2}^{T}\overset{(4)}{\mathbf{K}}{}_{S12}^{(3)T}\Big)\delta\mathbf{Q}_{W1}\\&-\Big(\mathbf{Q}_{V1}^{T}\overset{(1)}{\mathbf{K}}{}_{S12}^{(3)}+\mathbf{Q}_{V2}^{T}\overset{(1)}{\mathbf{K}}{}_{S2}^{(3)}+\mathbf{Q}_{W1}^{T}\overset{(2)}{\mathbf{K}}{}_{S12}^{(3)}+\mathbf{Q}_{W2}^{T}\overset{(2)}{\mathbf{K}}{}_{S2}^{(3)}+\dot{\mathbf{Q}}_{V1}^{T}\overset{(3)}{\mathbf{K}}{}_{S12}^{(3)}+\dot{\mathbf{Q}}_{V2}^{T}\overset{(3)}{\mathbf{K}}{}_{S2}^{(3)}\\&+\dot{\mathbf{Q}}_{W1}^{T}\overset{(4)}{\mathbf{K}}{}_{S12}^{(3)}+\dot{\mathbf{Q}}_{W2}^{T}\overset{(4)}{\mathbf{K}}{}_{S2}^{(3)}\Big)\delta\mathbf{Q}_{V2}\\&-\Big(\mathbf{Q}_{W1}^{T}\overset{(1)}{\mathbf{K}}{}_{S12}^{(3)}+\mathbf{Q}_{W2}^{T}\overset{(1)}{\mathbf{K}}{}_{S2}^{(3)}-\mathbf{Q}_{V1}^{T}\overset{(2)}{\mathbf{K}}{}_{S12}^{(3)}-\mathbf{Q}_{V2}^{T}\overset{(2)}{\mathbf{K}}{}_{S2}^{(3)}+\dot{\mathbf{Q}}_{W1}^{T}\overset{(3)}{\mathbf{K}}{}_{S12}^{(3)}+\dot{\mathbf{Q}}_{W2}^{T}\overset{(3)}{\mathbf{K}}{}_{S2}^{(3)}\\&-\dot{\mathbf{Q}}_{V1}^{T}\overset{(4)}{\mathbf{K}}{}_{S12}^{(3)}-\dot{\mathbf{Q}}_{V2}^{T}\overset{(4)}{\mathbf{K}}{}_{S2}^{(3)}\Big)\delta\mathbf{Q}_{W2}\\\equiv&\,\mathbf{R}_{V1}^{T}\delta\mathbf{Q}_{V1}+\mathbf{R}_{W1}^{T}\delta\mathbf{Q}_{W1}+\mathbf{R}_{V2}^{T}\delta\mathbf{Q}_{V2}+\mathbf{R}_{W2}^{T}\delta\mathbf{Q}_{W2},\end{aligned}$$

where the element matrices are listed in Appendix C.

APPENDIX C: ELEMENT MATRICES

$$\mathbf{M}_{S1}=\int_0^S\rho_S(A_S\mathbf{\Phi}_{S1}^{T}\mathbf{\Phi}_{S1}+I_S\mathbf{\Phi}_{S1}^{\prime T}\mathbf{\Phi}_{S1}^{\prime})\,\mathrm{d}x+\sum_{i=1}^{M}(m_{Di}\mathbf{\Phi}_{S1}^{T}|_{di}\mathbf{\Phi}_{S1}|_{di}+J_{Dyi}\mathbf{\Phi}_{S1}^{\prime T}|_{di}\mathbf{\Phi}_{S1}^{\prime}|_{di}),$$

$$\mathbf{M}_{S2}=\int_0^S\rho_S A_S\mathbf{\Phi}_{S2}^{T}\mathbf{\Phi}_{S2}\,\mathrm{d}x+\sum_{i=1}^{M}m_{Di}\mathbf{\Phi}_{S2}^{T}|_{di}\mathbf{\Phi}_{S2}|_{di},$$

$$\mathbf{M}_{S12} = \int_0^S \rho_S A_S \mathbf{\Phi}_{S1}^T \mathbf{\Phi}_{S2}\,\mathrm{d}x + \sum_{i=1}^{M} m_{Di} \mathbf{\Phi}_{S1}^T|_{di} \mathbf{\Phi}_{S2}|_{di},$$

$$\mathbf{M}_{Di} = \pi \rho_D h_{Di} \int_{a_{0i}}^{b_{0i}} \mathbf{\Phi}_{Di}^T \mathbf{\Phi}_{Di} r\,\mathrm{d}r, \quad \mathbf{M}_{SDi} = \pi \rho_D h_{Di} \mathbf{\Phi}_{S1}'^T|_{di} \int_{a_{0i}}^{b_{0i}} \mathbf{\Phi}_{Di} r^2\,\mathrm{d}r,$$

$$\mathbf{K}_{S1}^{(1)} = \int_0^S \rho_S (A_S \mathbf{\Phi}_{S1}^T \mathbf{\Phi}_{S1} - I_S \mathbf{\Phi}_{S1}'^T \mathbf{\Phi}_{S1}')\,\mathrm{d}x + \sum_{i=1}^{M} m_{Di} \mathbf{\Phi}_{S1}^T|_{di} \mathbf{\Phi}_{S1}|_{di} + \sum_{i=1}^{M} (J_{Dyi} - J_{Dxi}) \mathbf{\Phi}_{S1}'^T|_{di} \mathbf{\Phi}_S'|_{di},$$

$$\mathbf{K}_{S1}^{(2)} = \int_0^S (E_S I_S \mathbf{\Phi}_{S1}''^T \mathbf{\Phi}_{S1}'')\,\mathrm{d}x, \quad \mathbf{K}_{S2}^{(2)} = \int_0^S (k G_S A_S \mathbf{\Phi}_{S2}'^T \mathbf{\Phi}_{S2}')\,\mathrm{d}x,$$

$$\overset{(j)}{\mathbf{K}}_{S1}^{(3)} = \sum_{i=1}^{N} e_{ij} \mathbf{\Phi}_{S1}^T|_{bi} \mathbf{\Phi}_{S1}|_{bi}, \quad \overset{(j)}{\mathbf{K}}_{S2}^{(3)} = \sum_{i=1}^{N} e_{ij} \mathbf{\Phi}_{S2}^T|_{bi} \mathbf{\Phi}_{S2}|_{bi}, \quad \overset{(j)}{\mathbf{K}}_{S12}^{(3)} = \sum_{i=1}^{N} e_{ij} \mathbf{\Phi}_{S1}^T|_{bi} \mathbf{\Phi}_{S2}|_{bi},$$

$$j = 1, 2, 3, 4,$$

$$\mathbf{K}_{Di} = \pi \int_{a_{0i}}^{b_{0i}} \left\{ D_i r \mathbf{\Phi}_{Di}''^T \mathbf{\Phi}_{Di}'' + 2 D_i \nu_D \mathbf{\Phi}_{Di}''^T \mathbf{\Phi}_{Di}' + \left(N_r r + \frac{D_i (3 - 2\nu_D)}{r} \right) \mathbf{\Phi}_{Di}'^T \mathbf{\Phi}_{Di}' - \frac{2 D_i \nu_D}{r} \mathbf{\Phi}_{Di}''^T \mathbf{\Phi}_{Di} - \frac{2 D_i (3 - 2\nu_D)}{r^2} \mathbf{\Phi}_{Di}'^T \mathbf{\Phi}_{Di} + \left(\frac{N_\theta}{r} + \frac{D_i (3 - 2\nu_D)}{r^3} \right) \mathbf{\Phi}_{Di}^T \mathbf{\Phi}_{Di} \right\} \mathrm{d}r,$$

where

$$e_{i1} = k_{i1} + c_{i2}\Omega, \quad e_{i2} = k_{i2} - c_{i1}\Omega, \quad e_{i3} = c_{i1}, \text{ and } e_{i4} = c_{i2},$$

and $|_{di}$ represents values evaluated at the ith disk location. A prime represents differentiation with respect to the spatial variables x and r for $\mathbf{\Phi}_S$ and $\mathbf{\Phi}_{Di}$, respectively.

APPENDIX D: NOMENCLATURE

a, a_{0i}	disk inner-clamping radius
A_S	cross-sectional area of the shaft
b, b_{0i}	disk outer radius
b_i	locations of bearings on the shaft
c_{i1}, c_{i2}	radial damping coefficients of bearings
D, D_i	flexural rigidity of disks
d_i	locations of disks on the shaft

E, E_S, E_D	Young's moduli
F_p	inertia force of a vibrating disk
G_S	shear modulus
h_D, h_{Di}	thickness of disks
I_S	area moment of inertia of the shaft about a diameter
J_{Dxi}	disk mass moment of inertia about the axis of rotation
J_{Dyi}	disk mass moment of inertia about a diameter
k	shear correction factor
k_{i1}, k_{i2}	radial stiffness coefficients of bearings
L	Lagrangian
M	total number of disks
M_p	inertia moment of a vibrating disk
m_{Di}	mass of a disk
(m, n)	disk mode with m nodal diameters and n nodal circles
N	number of bearings
N_0	number of degrees of freedom of the total discretized system
N_r, N_θ	normal stress resultants in polar co-ordinates
q_k	generalized independent co-ordinates
$\mathbf{Q}_{\xi i}$, $\mathbf{Q}_{\eta i}$, $\mathbf{Q}_{Vi}$, $\mathbf{Q}_{Wi}$	column vectors consisting of generalized co-ordinates
(r, θ)	polar co-ordinates for a disk
R_k	generalized forces from bearing action
R_{mn}	radial distribution of disk mode shapes
S	length of the shaft
T, T_D, T_{Di}, T_S	kinetic energies
u_D, u_{Di}	transverse displacements of disks
V, V_D, V_{Di}, V_S	potential energies
(v_S, w_S), (V_S, W_S)	total transverse displacements of the shaft
(v_{S1}, w_{S1})	flexural deformations of the shaft
(v_{S2}, w_{S2})	shearing deformations of the shaft
δW	virtual work done by the bearing forces
$\mathbf{Z}_{Di}$, $\mathbf{Z}_{S1}$, $\mathbf{Z}_{S2}$	column vectors consisting of generalized co-ordinates of complex form
$\mathbf{\Phi}_{Di}$, $\mathbf{\Phi}_{S1}$, $\mathbf{\Phi}_{S2}$	row vectors consisting of admissible functions
ρ, ρ_D, ρ_S	mass densities
v, v_D	Poisson's ratios
∇^2	Laplacian operator
∇^4	biharmonic operator
Ω	rotational speed of the shaft
θ_{mn0}	orientation angle of a disk mode

Subscripts

bi, *di*	values evaluated at the *i*th bearing and *i*th disk location
D	disk
Di	*i*th disk
S	shaft